Biochimica et Biophysica Acta 1827 (2013) 520–528

Contents lists available at SciVerse ScienceDirect

Biochimica et Biophysica Acta

journal homepage: www.elsevier.com/locate/bbabio

Study of cell-differentiation and assembly of photosynthetic proteins during greening of etiolated *Zea mays* leaves using confocal fluorescence microspectroscopy at liquid-nitrogen temperature

Yutaka Shibata *, Wataru Katoh, Yukari Tahara

Division of Material Science (Physics), Graduate School of Science, Nagoya University, Nagoya 464-8602, Japan

ARTICLE INFO

Article history:
Received 29 November 2012
Received in revised form 31 January 2013
Accepted 6 February 2013
Available online 14 February 2013

Keywords:
Prolamellar body
Prothylakoid
C4-plant
Protochlorophyllide

ABSTRACT

Fluorescence microspectroscopy observations were used to study the processes of cell differentiation and assemblies of photosynthesis proteins in *Zea mays* leaves under the greening process. The observations were done at 78 K by setting the sample in a cryostat to avoid any undesired progress of the greening process during the measurements. The lateral and axial spatial resolutions of the system were 0.64 μm and 4.4 μm, respectively. The study revealed the spatial distributions of protochlorophyllide (PChld) in both the 632-nm-emitting and 655-nm-emitting forms within etiolated *Zea mays* leaves. The sizes of the fluorescence spots attributed to the former were larger than those of the latter, validating the assignment of the former and latter to the prothylakoid and prolamellar bodies, respectively. *In vivo* microspectroscopy observations of mature *Zea mays* leaves confirmed the different photosystem II (PS I)/photosystem I (PS II) ratio between the bundle sheath (BS) and mesophyll (MS) cells, which is specific for C4-plants. The BS cells in *Zea mays* leaves 1 h after the initiation of the greening process tended to show fluorescence spectra at shorter wavelength side (at around 679 nm) than the MS cells (at around 682 nm). The 679-nm-emitting chlorophyll-*a* form observed mainly in the BS cells was attributed to putative precursor complexes to PS I. The BS cells under 3-h greening showed higher relative intensities of the PS I fluorescence band at around 735 nm, suggesting the reduced PS II amount in the BS cells in this greening stage.

1. Introduction

When angiosperms are germinated under dark, the seedlings have leaves with a pale yellow color. Cells in these "etiolated" leaves contain etioplasts, which are precursors to the chloroplasts and accumulate a late chlorophyll (Chl) intermediate, protochlorophyllide (PChld). Since the accumulation of Chl is requisite for the accumulation of most of photosynthetic proteins, their content in an etioplast is generally limited at a very low level [1–4]. Irradiation to an etiolated seedling induces the greening process, through which photosynthetic apparatuses are developed. The mechanisms of coordinated biogenesis and assemblies of the photosynthesis proteins during the greening process largely remain to be established.

Early studies using electron microscopes (EMs) have clarified temporal changes in the microscopic morphology of etioplasts during the greening process [5–8]. These studies have shown that an etioplast contains a particle called a prolamellar body (PLB) with a typical diameter of several hundreds of nanometers. The studies have also identified another membranal structure in an etioplast called prothylakoid (PT), which radially extends from PLB. PLB and PT are composed of a continuous membrane system containing PChld, several kinds of lipids, and polypeptides. They are both precursors to the thylakoid membrane. During continuous illumination, the granular structure of PLB diminishes within several hours [5] and the mature thylakoid membrane is formed in 24 h to 96 h [9,10].

Since the pioneering work by Shibata [11], studies using the fluorescence spectroscopy have been powerful tools to identify the assembly intermediates of photosynthetic pigment-protein complexes with characteristic spectral properties during the greening process [10,12,13]. Most PChld contained in an etioplast is in either of two forms with emission maxima at 632 nm ($PChld_{632}$, hereafter) and 655 nm ($PChld_{655}$, hereafter) [14,15]. The latter is known to be the photoactive form and is considered to be comprised of the PChld aggregated form involving

Abbreviations: Chl, chlorophyll; PChld, protochlorophyllide; EM, electron microscope; PLB, prolamellar body; PT, prothylakoid; RC, reaction center; PS II, photosystem II; PS I, photosystem I; NADPH, nicotinamide adenine dinucleotide phosphate; BS, bundle sheath; MS, mesophyll; CCD, charge-coupled device; VB, vascular bundle; PSF, point spread function; LHC, light-harvesting complex

* Corresponding author at: Department of Chemistry, Graduate School of Science, Tohoku University, Aramaki aza Aoba, Aoba-ku, Sendai 980-8578, Japan. Tel.: +81 22 795 6568; fax: +81 22 795 6570.
E-mail address: shibata@m.tohoku.ac.jp (Y. Shibata).

0005-2728/$ – see front matter © 2013 Elsevier B.V. All rights reserved.
http://dx.doi.org/10.1016/j.bbabio.2013.02.001

NADPH–Pchld-oxidoreductase, the enzyme catalyzing the photoconversion of PChld. A short flash illumination to an etiolated leaf causes an immediate transformation of the photoactive $PChld_{655}$ into chlorophyllide, as observed from the rapid emergence of the fluorescence peak at 688 nm and concomitant decrease of the 655-nm fluorescence band [16]. This primary event is followed by parallel fluorescence peak shifts to 695 nm and to 675 nm. The major fluorescence band at 695 nm then shows a shift to 682 nm under dark, which is known as the Shibata shift [11,16,17].

Recent genetic studies using mutant screenings of cyanobacteria, green algae, and higher plants have identified an increasing number of auxiliary proteins assisting the assemblies of photosynthetic proteins [18–20]. These studies are shedding light on a complicated regulation network of these auxiliary proteins ensuring the coordinated biogenesis of photosynthetic proteins. Biochemical analyses have also been conducted to clarify the sequences of the assembly steps involving these auxiliary proteins [21–23]. According to Rokka et al. [21], the first detectable intermediate of the photosystem II (PS II) assembly is composed of D1–D2–Cytb559, *i.e.*, the complex called the PS II-reaction center (RC). The core antenna subunit CP47 is then assembled into the complex, and the assemblies of CP43 and other small subunits follow. There have been only a limited number of reports about the assembly intermediates of photosystem I (PS I). Ozawa et al. [23] succeeded in purifying an intermediate assembly complex of PS I comprising subunits PsaA to Psa F and some other small subunits. An auxiliary protein, Ycf4, was found to be involved in the PS I assembly intermediate [22].

The optical microscope that can resolve the localization of each assembly intermediate mentioned above will be a powerful tool to reveal the intracellular temporal sequence of the assembly steps of photosynthetic proteins. Such microspectroscopic studies will help integrate the accumulated knowledge about the intermediate assembly forms, the dynamical morphology changes observed by EM, the auxiliary proteins, and their network during the greening process. $PChld_{655}$ and $PChld_{632}$ have been assigned to be respectively emitted from PLB and PT based on measurements of the fluorescence spectra of biochemically isolated PLB and PT [24]. Spectral measurements of the intact etiolated leaves with an optical microscope will give a direct validation of the above assignment. Several research groups have shown that the localization of PS II within granal regions of a chloroplast can be spatially resolved with optical microscope techniques using confocal excitation [25,26] and two-photon excitation [27]. Nevertheless, there have been only limited studies using an optical microscope technique to study the light-induced development of the photosynthetic systems in etioplasts [28,29]. Major difficulties in applying microspectroscopy to observations of leaves under the greening process are in the rapid developments of etiolated leaves under light, which make detailed spectroscopic measurements critically difficult.

To apply the microspectroscopic technique to observations of the maturation process during the greening process, we carried out microscope observations of etiolated leaf specimens at cryogenic temperatures to suppress any undesired development of the photosynthetic systems during measurements. We used a conventional laser-scanning confocal microscope equipped with an optical cryostat and a polychromator. The samples were sectioned leaves from etiolated or greening seedlings of maize, *Zea mays*, which is known to be a C4-plant. Leaves of a C4-plant have differentiated bundle sheath (BS) and mesophyll (MS) cells containing chloroplasts with different PS II/PS I ratios. The BS cells of a C4-plant have significantly low PS II contents, which ensure their efficient CO_2 fixation in the Calvin cycle because the activity of Rubisco is highly sensitive to the oxygen partial pressure. The microscope set-up in the present study has sufficient spatial resolution to resolve the BS and MS cells. Thus, selective observations of the BS cells will give opportunities to observe the development of PS I with reduced interferences with PS II components.

2. Materials and methods

2.1. Organisms and growth conditions

Etiolated *Zea mays* seedlings were grown on vermiculite moistened with tap water for eight days in the dark at 18 °C. Mature maize seedlings were grown in 8-day cycles of a regime of 14 h in the light at 23 °C and 10 h in the dark at 21 °C. Greening of etiolated leaves was triggered by irradiation of 11,000-lx stationary light from a fluorescent lamp to an etiolated 8-day-old *Zea mays* seedling. Leaf sections were prepared by slicing the first leaves of the seedlings with a razor blade. The etiolated-leaf sections were prepared in the dim green light from an LED (LM-D2426G, ASAHI-DENKI, Osaka) to avoid any light-induced transformation during the specimen preparation.

Five-to-ten leaf sections were suspended in an aquatic solution supplemented with 67% (v/v) glycerol as antifreeze. The suspension was then sealed in a cavity between two quartz windows in a homemade copper sample holder, set in a flow-type cryostat (Microstat, Oxford Instruments, Eynsham), and cooled to 78 ± 1 K by a continuous cold nitrogen flow. The cryostat was set on the stage of a conventional laser-scanning confocal microscope (Nanofinder, Tokyo Instruments, Tokyo). The sample temperature was measured with a chromel-gold/iron thermocouple fixed on the surface of the sample holder. Measurements at the cryogenic temperature practically arrest the development of the greening process in etiolated and greening samples. They also prevent the occurrence of pigments in the samples from the photo-damage caused by intense laser irradiations.

2.2. Microspectroscopy set-up

The frequency-doubled light at 445 nm from a mode-locked Ti: sapphire laser (MaiTai, Spectra-Physics, Mountain View) was used as an excitation light. The pulse duration and repetition rate of the laser were about 110 fs and 80 MHz, respectively. The typical excitation power used was 15 μW. A pair of galvano-mirrors was used for the scanning of the laser focus point on the sample. The laser light was focused onto the sample with an objective lens (Plan Fluor ELWD ×40, numerical aperture (NA) 0.60, Nikon, Tokyo). The fluorescence was collected with the same objective lens, passed through a dichroic mirror and a long-pass filter, and focused onto the entrance slit of the polychromator. The fluorescence signal was detected using a cooled back-illuminated CCD detector (DU420-BV, Andor Technology, Belfast). The pixel size was 1 μm × 1 μm unless it is explicitly stated. The accumulation time for each pixel was 20 ms for greening and mature leaf sections, while it was 100 ms for etiolated-leaf sections to obtain sufficient signal/noise ratio due to their weak emission. Fluorescence images will be shown with neither de-convolution nor interpolation between pixels throughout this article.

In the present set-up, each pixel in a fluorescence image does not contain full spectrum information, instead includes the integrated counts over up-to 3 independent spectral ranges that can be arbitrarily selected. When we measure a full fluorescence spectrum emitted from a selected position on a fluorescence image obtained beforehand, the galvano-mirrors were manipulated to move the laser spot as desired. The fluorescence spectrum obtained as above was attributed to the limited volume in the sample that has almost the same size as that of the point spread function (PSF) of the system. Hereafter, we call this type of fluorescence spectra "microscopic fluorescence spectra". The spatial resolution of the present set-up is defined as the full width at half maximum (FWHM) of PSF and was experimentally estimated from microscope observations of fluorescent beads with a diameter of 0.2 μm spin-coated on a cover glass. The spatial resolution depended on the size of the confocal pinhole set at the entrance of the polychromator. In the present study, we used the square pinhole with a size of 0.03 mm. The lateral and axial spatial resolution of the

present set-up was estimated to be 0.64 μm and 4.4 μm, respectively. This slit width gave a spectral resolution of ca. 1.0 nm.

3. Results

3.1. Microscopic distributions of photosystems in mature Zea mays leaves

Fig. 1 (A) and (B) shows typical fluorescence images of a sectioned mature leaf of *Zea mays* at 78 K. The scale bar represents 40 μm. The image in panel (A) was reconstructed using the fluorescence signal accumulated over the 680–690-nm spectral range, which is mainly emitted from PS II and hereafter designated "$Fl_{PS\ II}$." The image in panel (B), on the other hand, was reconstructed using the PS I fluorescence over the 725–735-nm spectral range, which is hereafter designated "$Fl_{PS\ I}$." The images in Fig. 1 are the views from a roughly parallel direction to the vascular bundle (VB). In these images, cell boundaries were generally not clear because non-fluorescent cell walls were not visible. Nevertheless, bright areas in the images seemed to be separated into many parts, in which several bright spots were clustering. Each cluster may correspond to an individual cell, and each bright spot within a cluster may be an individual chloroplast. VB is observed as a dark hole around the center surrounded by the bright clusters. The BS cells are the clusters peripheral to VB, while the MS cells are those located outside the nearest neighbor cells to VB. Typical microscopic fluorescence spectra are shown in Fig. S1 in Supplementary materials. We took generally one microscopic spectrum per single cell that could be recognized as a cluster of bright spots as shown in Fig. 1. These spectra showed a smaller PS I fluorescence band at around 735 nm than those of a living leaf observed by a conventional fluorometer. The prominent 695-nm band, which is specific for the isolated PS II preparation, was also absent in the microscopic spectra. These apparent discrepancies might be explained by a reduced self-absorption effect under the microscope measurements.

Although the cell boundaries were not clear in the images, we could observe the cell differentiation into the BS and MS cells with different optical properties, which is specific for C4-plants like maize. Fig. 1(C) shows the fluorescence-ratio map constructed using the images in panels (A) and (B). Each pixel in the image in Fig. 1(C) contains the ratio $Fl_{PS\ II}/Fl_{PS\ I}$ of the corresponding pixel in the images in panels (A) and (B), except for those in which fluorescence signals are less than a certain threshold value. The threshold was introduced to avoid divergent results due to divisions by tiny values. The map indicated that the nearest neighboring cells to VB tended to show lower ratio values than those located outside, suggesting decreased PS II/PS I ratios in BS cells. In Fig. 1(D), the plots of $Fl_{PS\ II}$ *vs.* $Fl_{PS\ I}$ are compared among several regions indicated by the boxes in panel (C). The pixels in the BS cells showed almost the same PS I fluorescence levels and significantly reduced PS II fluorescence levels, suggesting that the decreases in the PS II/PS I ratio in BS cells are mainly due to the suppression of the PS II content. These observations were reproducible among independent preparations of the mature leaf sections.

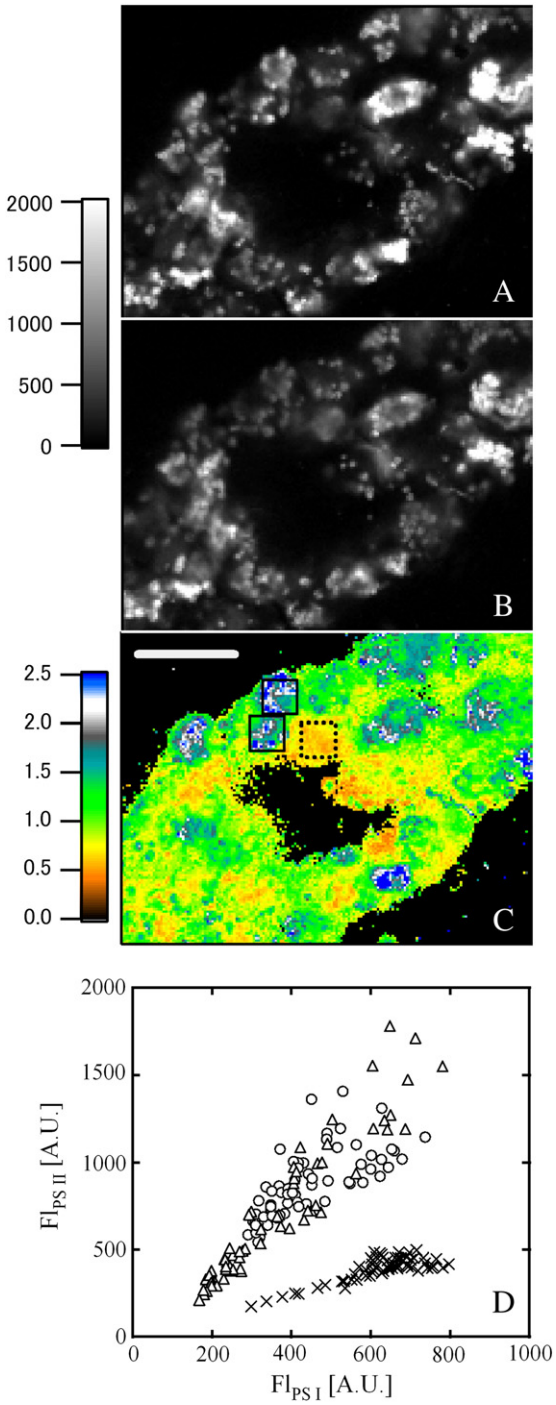

Fig. 1. Typical fluorescence microscope images of a sectioned mature *Zea mays* leaf monitored in the PS II fluorescence region (680–690 nm) (A) and in the PS I fluorescence region (725–735 nm) (B) at 78 K. Fluorescence-ratio map (C) of the intensities in the PS II region to those in the PS I region. The scale bar represents 40 μm. The fluorescence intensity in the PS II region is plotted against that of the PS I region (D) in each pixel within the boxes with solid lines (open circles and open triangles) and the box with a dotted line (crosses) in panel C.

3.2. Pigment distributions in etiolated Zea mays leaves

Fig. 2 shows 78-K fluorescence images of a sectioned etiolated leaf of *Zea mays*. The scale bar represents 5 μm. It should be noted that the images in Fig. 2 were represented with a magnified scale as compared with those in Fig. 1. Reduced-magnification images are also shown in Fig. S2 in Supplementary materials. The image in panel (A) was reconstructed using the 632-nm fluorescence, and that in panel (B), using the 655-nm fluorescence. Each bright spot in panels (A) and (B) indicates an individual etioplast, which contains PChld in the 632-nm-emitting form ($PChld_{632}$, hereafter) mainly in PT and in the 655-nm-emitting form ($PChld_{655}$, hereafter) mainly in PLB. We confirmed that the microscopic fluorescence spectra at typical bright spots showed peaks at 632 nm and 655 nm (typical fluorescence spectra are shown in Fig. S3 in Supplementary materials). The images in Fig. 2 clearly indicated larger spot sizes for $PChld_{632}$ than for $PChld_{655}$. The larger spot sizes for $PChld_{632}$ than for $PChld_{655}$ are also apparent in the fluorescence images with a reduced magnification (Fig. S2), in which many fluorescence spots observed in the 628–638 nm region look more blurry than those

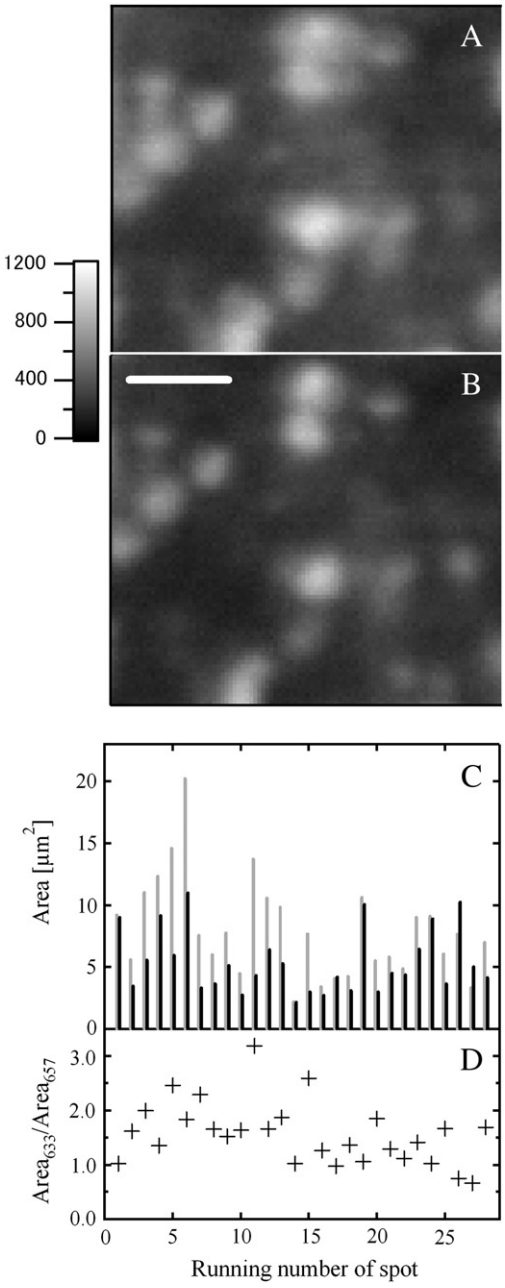

Fig. 2. Typical fluorescence microscope images of a sectioned etiolated *Zea mays* leaf monitored in the PT fluorescence region (628–638 nm) (A) and in the PLB fluorescence region (652–662 nm) (B) at 78 K. The pixel size was 0.2 μm × 0.2 μm and the scale bar represents 5 μm. The gray and black bars in (C) show the estimated areas of the fluorescence spots monitored in the 628–638-nm and the 652–662-nm spectral regions, respectively. The ratios, $Area_{632}/Area_{655}$, are shown with crosses in (D). The horizontal axis of panels (C) and (D) shows the running number arbitrarily given to individual spots.

in the 652–662 nm region. This observation is consistent with the assignment based on the biochemical isolation technique [24].

To evaluate the sizes of the bright spots in Fig. 2 more quantitatively, we fitted individual spots to 2-dimensional Gaussian functions,

$$Fl(x,y) = A_0 + A\exp\left[\frac{-1}{2(1-cor^2)}\left\{\left(\frac{x-x_0}{\sigma_x}\right)^2 + \left(\frac{y-y_0}{\sigma_y}\right)^2 - \frac{2cor(x-x_0)(y-y_0)}{\sigma_x\cdot\sigma_y}\right\}\right] \quad (1)$$

Here, A_0 is the parameter to adjust the background. The contour line at one-half of the maximum value A forms an ellipse. The size of the spot was evaluated from the area of the ellipse,

$$Area = \pi\sqrt{2\ln 2}\cdot\sigma_x\cdot\sigma_y \quad (2)$$

In Fig. 2(C), we show the estimated spot areas for $PChld_{632}$ (gray bars on left) and for $PChld_{655}$ (black bars on right), indicating larger sizes of $PChld_{632}$ spots. Fig. 2(D) shows the area ratios of the spots of $PChld_{632}$ to those of $PChld_{655}$, which were significantly larger than unity. The estimated average value of the ratio was 1.57 with its standard deviation of 0.57. Unfortunately, we could not control slight deviations of the positions of individual etioplasts from the focal plane. These deviations may result in the large standard deviation of the ratio values shown with crosses in Fig. 2(D).

3.3. Microscope imaging of 1-h greening Zea mays leaves

We also observed confocal microscope images of sectioned *Zea mays* leaves under the greening process. The first leaf was harvested from a seedling during the greening process induced by stationary light irradiation. Leaf sections were prepared by slicing the leaf with a razor blade under light, immediately setting them in the sample holder of the cryostat, and cooling to 78 K. Approximately 10 min was required for the above procedure. The sample temperature fell below 200 K within ca. 10 min of the specimen setting. Because greening proceeds during specimen preparation, hereafter, we call the leaf section sample harvested 50 min and 170 min after the start of the greening-inducing light irradiation "1-h greening leaf" and "3-h greening leaf," respectively.

Fig. 3 shows typical normalized microscopic fluorescence spectra at randomly selected locations of the 1-h greening *Zea mays* leaf sections. The peak wavelengths of the microscopic spectra varied from 678 nm to 685 nm. Such a large dispersion in the fluorescence peak wavelength was not observed in the mature leaf samples (see Fig. S1). The observed large peak-wavelength dispersion suggests the existence of multiple

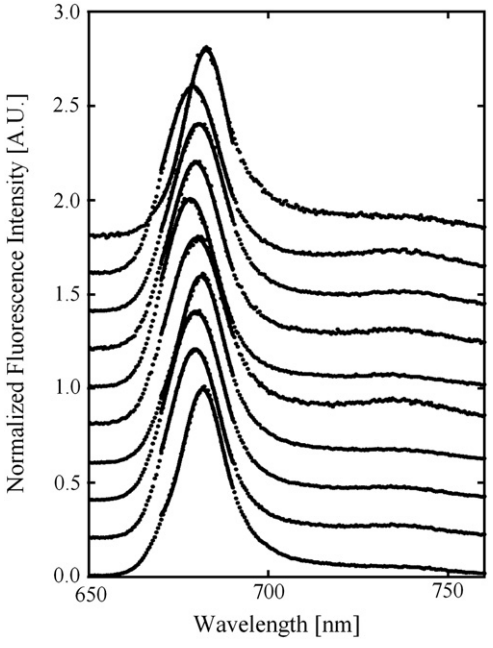

Fig. 3. Typical microscopic fluorescence spectra at randomly selected locations of sectioned *Zea mays* leaves 1 h after the start of the greening process. The heights of the spectra are normalized to unity. The solid lines show the fitting curves to Gaussian functions.

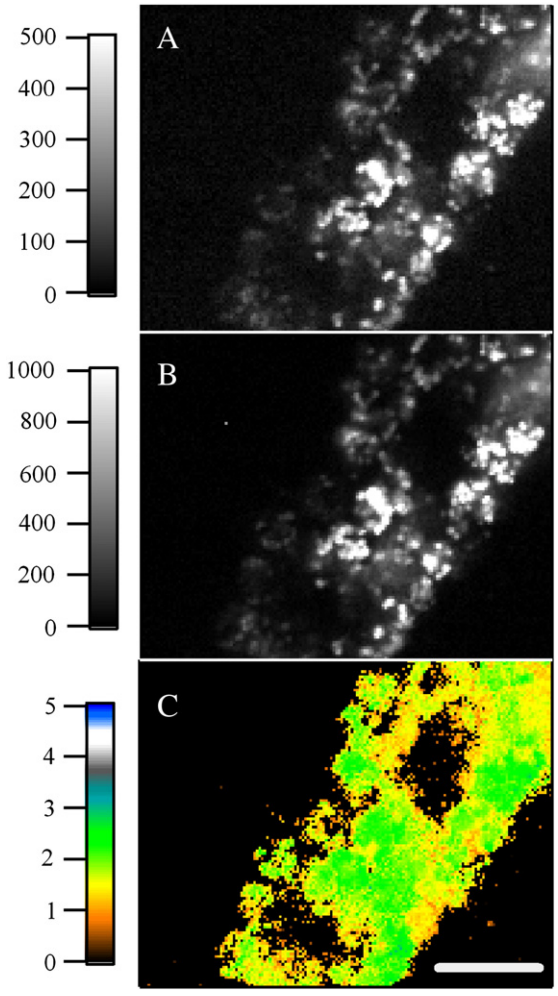

Fig. 4. Typical fluorescence microscope images of a sectioned 1-h greening *Zea mays* leaf monitored in the shorter-wavelength side (670–680 nm) (A) and in the longer-wavelength side (680–690 nm) (B) at 78 K. Fluorescence-ratio map (C) of the intensity in the longer wavelength side (680–690 nm) to that of the shorter wavelength side (670–680 nm). The scale bar represents 40 μm.

Chl-*a* forms with different optical properties. Fluorescence spectra having shorter peak wavelengths tended to have larger spectral widths.

Fig. 4(A) and (B) shows typical fluorescence images of a sectioned 1-h greening *Zea mays* leaf at 78 K. To visualize different distributions between the shorter-wavelength-emitting and the longer-wavelength-emitting Chl-*a* forms, we obtained images using the fluorescence signal accumulated over the 670–680-nm range (hereafter $Fl_{670-680}$, panel A) and over the 680–690-nm range (hereafter $Fl_{680-690}$, panel B). These images were viewed from a roughly parallel direction to VB, which appeared as a dark hole surrounded by bright clusters.

To more clearly visualize the different distributions, we show the fluorescence-ratio maps in Fig. 4(C). The map is the ratio of the $Fl_{680-690}$ image (Fig. 4B) to the $Fl_{670-680}$ image (Fig. 4A). As shown in Fig. 3, the peak wavelengths of the microscopic fluorescence spectra of the 1-h greening leaves lie at around 680 nm in average. Thus, small peak shifts of microscopic spectra from 680 nm are expected to be well reflected on the ratio map. At present, we could obtain ratio maps including the pigment distributions around VB for three independent sections. The other two are shown in Fig. S4 in Supplementary materials. Unfortunately, the number of samples is rather small, because it is difficult to stably prepare thin sections of 1-h greening leaves that face their VB parallel to the optical axis. The comparison of the three ratio maps in Figs. 4 and S4 suggests that the ratio always has a low value in the peripheral region to VBs, although some stochastic fluctuation in the ratio value exists. On the other hand, regions distant from the VB showed relatively high ratio values with some exceptions, for example, in the regions near leaf surface. Thus, it can be said that the BS cells in the 1-h greening leaves tended to have fluorescence peaks at shorter wavelengths, while the MS cells tended to have them at longer wavelengths. Differentiation into BS and MS cells with different optical properties was already in progress 1 h after the start of the greening process.

3.4. Microscope imaging of 3-h greening Zea mays leaves

In Fig. 5, typical microscopic fluorescence spectra are compared at randomly selected locations of the 3-h greening *Zea mays* leaf sections. The electron-transfer active PS I and PS II complexes are known to have been formed already in this phase of greening, although the degree is still very limited [30–32]. The peak height of the fluorescence band at around 685 nm was normalized to unity. The relative intensities of the PS I fluorescence band at around 735 nm varied among the microscopic spectra, suggesting a strong dependence of the PS II/PS I ratio on the cell position. The large dispersion in the relative intensity of the PS I fluorescence reflects the cell differentiation specific for C4-plants. On the other hand, the dispersion in the peak wavelength of the 685-nm fluorescence band was much smaller than that for the 1-h greening samples.

Typical fluorescence images of the 3-h greening *Zea mays* leaf section are shown in Fig. 6. The fluorescence images were monitored in the 680–690-nm spectral region (hereafter $Fl_{680-690}$, panel A) and in the 725–735-nm PS I spectral region (hereafter $Fl_{PS\ I}$, panel B). Fig. 6(C) shows the fluorescence-ratio map of $Fl_{680-690}$ (Fig. 6(A)) to $Fl_{PS\ I}$ (Fig. 6(B)). For the 3-h greening leaves, we could obtain ratio maps for three independent sections. The number of samples is again rather small, due to the difficulty in the stable preparations of thin sections. The other two maps are shown in Fig. S5 in Supplementary materials. The maps clearly revealed the lower $Fl_{680-690}/Fl_{PS\ I}$ ratio around VB. This was also confirmed by the plots of $Fl_{680-690}$ *vs.* $Fl_{PS\ I}$ within several regions of the ratio map as shown in Fig. 6(D). The slopes of the plots in Fig. 6(D) were much gentler in the nearest neighbor cells to VB, indicating

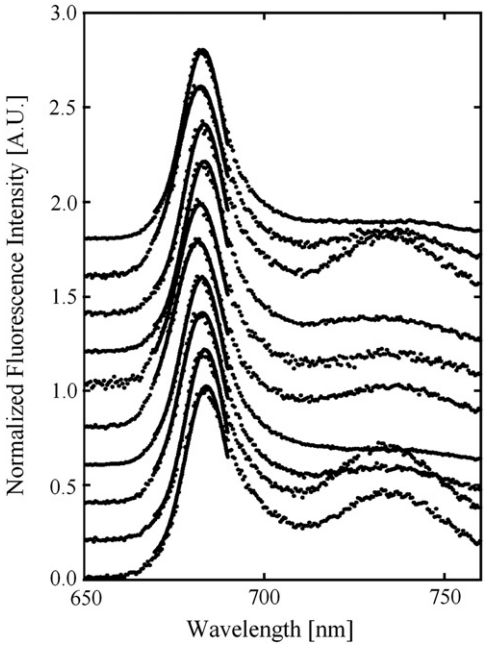

Fig. 5. Typical microscopic fluorescence spectra at randomly selected locations of sectioned 3-h greening *Zea mays* leaves. The heights of the spectra are normalized to unity. The solid lines show the fitting curves to Gaussian functions.

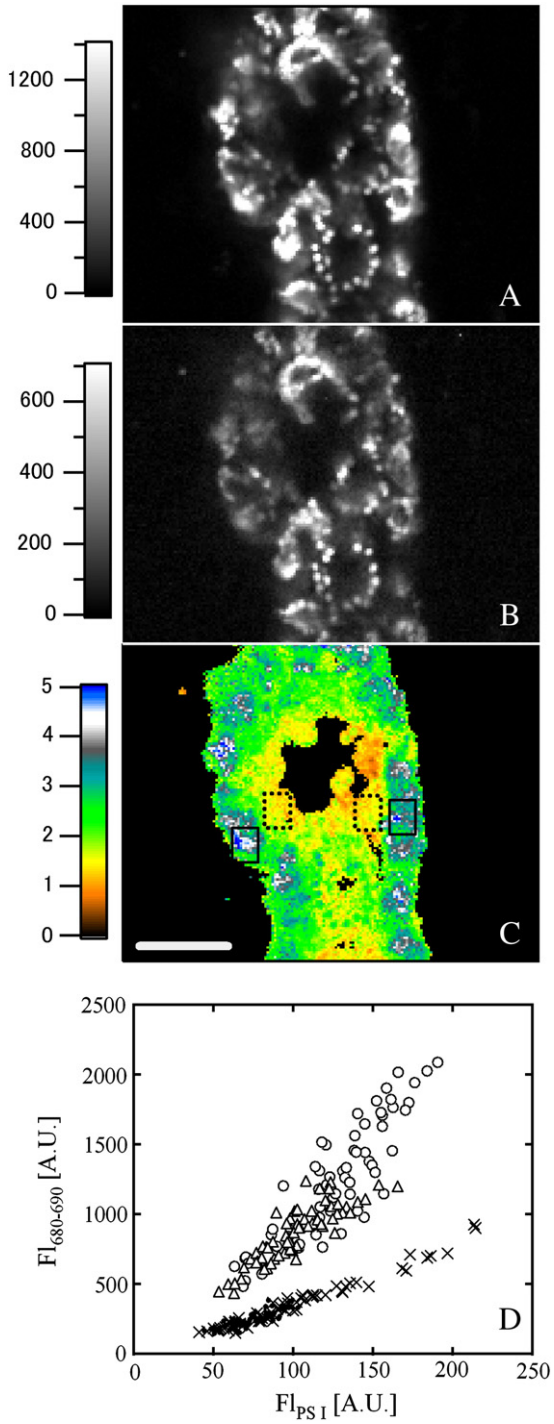

Fig. 6. Typical fluorescence microscope images of a sectioned 3-h greening *Zea mays* leaf monitored in the main fluorescence band (680–690 nm) (A) and in the PS I fluorescence region (725–735 nm) (B) at 78 K. Fluorescence-ratio map (C): intensity of the main band to that of the PS I band. The scale bar represents 40 μm. The fluorescence intensity of the main band is plotted against that of the PS I band (D) in each pixel within the boxes with solid lines (open circles and open triangles) and within the boxes with dotted lines (dots and crosses) in panel C.

roughly twofold higher $Fl_{680-690}/Fl_{PS\ I}$ ratios in the MS cells than in the BS cells. Fig. 6(D) also shows that BS and MS cells have comparable PS I fluorescence levels and that the lower $Fl_{680-690}/Fl_{PS\ I}$ ratios in the BS cells are due to the suppressed amount of the 685-nm-emitting Chl forms in the BS cells.

4. Discussion

4.1. Spatial resolution of the present study

Here, using confocal microspectroscopy at the cryogenic temperature, we could clarify different microscopic distributions of PChld/Chl-*a* in different states having different optical properties during the greening process. The observations could not be made without the use of the microscope imaging at the cryogenic temperature, where developments of the greening process could be practically arrested. The present set-up possessed only a limited spatial resolution especially for the axial direction, along which FWHM of PSF was about 4.4 μm. This value is somewhat larger than the theoretically estimated value of 4.2 μm according to the relation, $1.77\lambda n/(NA)^2$ with λ and *n* being the wavelength of light and the refractive index of the medium, respectively. The mechanical instabilities of the cryostat may slightly degrade the spatial resolution of the system. The spatial resolution of the present study was limited by the low NA value of the long working-distance objective lens, which could be used for observations through the windows of the cryostat.

In observations with such a low axial resolution, fluorescence from volumes adjacent to the focal plane is expected to contaminate the signal. Nevertheless, we could resolve the different distributions of pigments in the present study. This is partly because we selected leaf sections that happened to orient their VB axis parallel to the light axis. The cell characteristics will change with the distance from the VB but will not depend so much upon the position along the VB axis. Thus, the contamination of the background fluorescence would not degrade so much the lateral resolution. Conceivably, an improved spatial resolution is of primary importance, and, presently, we are engaged in improving the spatial resolution of the microscope at cryogenic temperatures.

4.2. Pigment distribution in PT and PLB

Blomqvist et al. [24] showed that isolated PLB and PT have fluorescence peak wavelengths at around 655 and 632 nm, respectively. The early EM images clarified a granular form of typical PLBs and typical structures of PT radially extending from PLB. The present microscope imaging of etiolated leaves revealed, for the first time, the larger size of the $PChld_{632}$ than the $PChld_{655}$ fluorescence spot *in vivo*. This observation was consistent with previous findings based on the biochemical isolation of PLB and PT and the EM observations. We expected to observe a dip around the center of the $PChld_{632}$ fluorescence spot, as indicated by the radial extension of PT from PLB and absence of $PChld_{632}$ in PLB. However, such a dip was not observed for the $PChld_{632}$ spots, probably because of the poor spatial resolution of the present set-up. To evaluate the effect of the poor resolution, we simulated the expected fluorescence images assuming model pigment distributions in PLB and PT. One has a spherical pigment distribution with a diameter of 1.2 μm (model for PLB), and the other has a spherical distribution with a diameter of 2.4 μm and a vacant core with a diameter of 1.2 μm (model for PT). All the spheres were assumed to be concentric. The expected fluorescence images were calculated by convolution of these model distributions with PSF of the present set-up. The above simulation confirmed that the dip was filled up after the convolution (data not shown).

4.3. Cell differentiation and assembly intermediates of photosystems

In the present study, we clearly resolved the different PS II/PS I ratios between the BS and MS cells by the microscope observations of sectioned mature *Zea mays* leaves. The PS II/PS I fluorescence ratio was confirmed to be lower in the BS than in the MS cells by an approximate factor of 4, which was quite consistent with the reported PS II/PS I ratio estimated by biochemical assays [33]. Fig. 1(D) clearly showed

that the low PS II/PS I ratio is mainly due to the suppression of the PS II content but not to the increased PS I level in the BS cells.

Fig. 5 demonstrates that 3-h illumination to an etiolated seedling induces a 735-nm fluorescence band. This observation is in line with the previous report by Dreyfuss and Thornber [34]. The fluorescence band at 735 nm is specific for PS I-LHC I or LHC I [35], while the PS I core complex deficient in its peripheral antennae has been considered to have a fluorescence peak at around 725 nm at 80 K [36]. Thus, here, we assume that the 735-nm fluorescence band observed for the 3-h greening leaves is emitted from the red-most Chl(s) in the PS I-LHC I complex or, possibly, free LHC I isolated from the PS I core complex. The amount of LHC I in this stage is still very low. Its fluorescence emission was observable in spite of the low amount probably because of its high fluorescence quantum yield at 78 K. At any rate, the observation clearly shows the formation of the mature PS I after 3-h continuous illumination.

Here, we assume that the relative intensity of the 735-nm fluorescence band is positively correlated with the level of the PS I core complex accumulation. The fluorescence-ratio map in Fig. 6(C) suggests that higher relative intensities of the 735-nm band were obtained in the cells peripheral to the VB while lower values were observed in the cells distant from the VB. This suggested that 3-h illumination to an etiolated seedling leads to differentiation into the BS and MS cells with different PS II/PS I ratios. Although the BS cells in the 3-h greening leaf showed 735-nm emission bands, their relative intensities were still lower than those observed for typical cells of a mature leaf (Fig. S1). This may reflect the fact that cells in this stage are still developing and the majority of Chls are associated with precursor complexes to the mature photosystems. The main fluorescence band at around 683 nm can be attributed to the precursor complexes.

The main fluorescence band of the 3-h greening leaf had a peak wavelength ranging from 680 to 684 nm. The contribution from mature PS II core complexes to this band should be only minor. This interpretation is based on the fact that the mature PS II core complex fully equipped with the core antennae, CP43 and CP47, has the characteristic emission with double peaks at 685 nm and 695 nm. The 695-nm band, which was emitted from CP47 [37–41], is absent in the spectra shown in Fig. 5. Although the microscopic fluorescence spectra of the mature leaf sections do not show prominent 695-nm bands (Fig. S1), their peak wavelengths are observed at much longer wavelength around 685 nm than those of the 3-h greening leaf. Thus, we assume that the majority of PS II in this 3-h greening stage is still in a form deficient in the mature core antennae and in a similar form to the so-called PS II–RC complex. This interpretation is in agreement with the observation by Rokka et al. [21] indicating that the first detectable intermediate of the PS II assembly has a similar subunit composition to that of PS II-RC.

The present study reveals larger variabilities of microscopic spectral profiles of the main band at around 680 nm for greening leaves than for mature leaves. A comparison of Fig. 3 with Fig. 5 suggests that the dispersion in the spectral properties of this main band is the largest for the 1-h greening leaf and decreases through the greening process. To evaluate the spectral variability more quantitatively, we fitted each microscopic spectrum to a Gaussian curve and estimated its band width and peak wavelength. The solid lines in Figs. 3, 5, and S1 show the fitting curves. The band width *vs.* peak wavelength plots of the microscopic spectra is shown in Fig. 7(B), which includes 143, 126, and 47 points for 1-h greening, 3-h greening, and mature leaf samples, respectively. All the microscopic spectra were measured at randomly selected 5 to 10 positions within a fluorescence image. We ensured the randomness of the selection by measuring one microscopic spectrum per single cell as long as we could recognize the cell boundary. Fig. 7(A) and (C) shows the distributions of the peak wavelengths and the widths of the microscopic spectra. These distributions

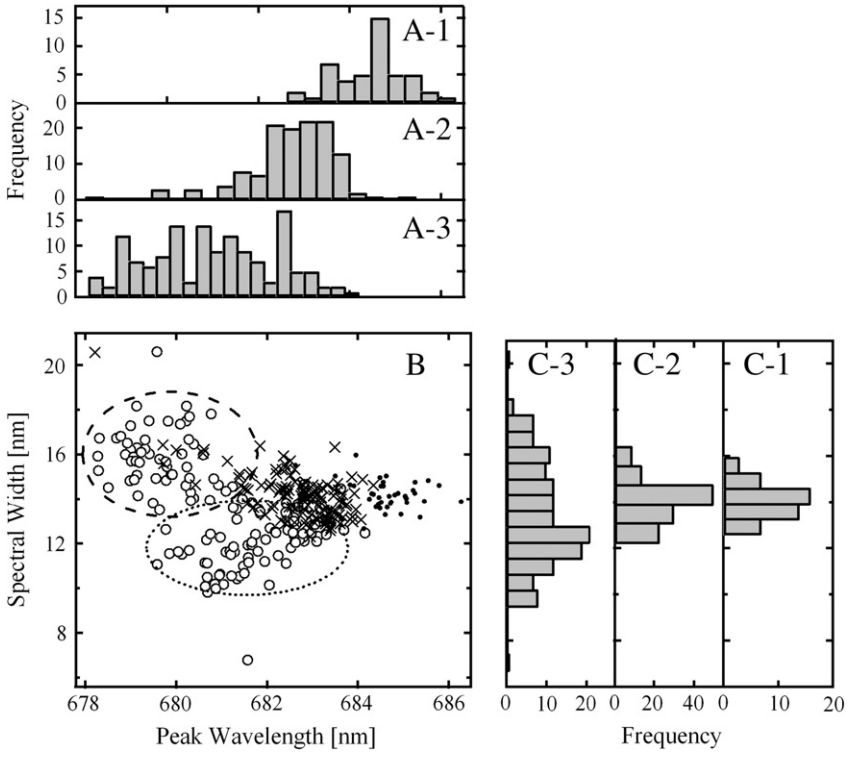

Fig. 7. The spectral widths of microscopic fluorescence spectra are plotted against their peak wavelengths (B). The values were estimated from the Gaussian fittings of the experimentally obtained spectra (see text) at randomly selected locations in the sectioned *Zea mays* leaves 1 h after the start of the greening process (open circles), 3 h after the start of the greening process (crosses), and in mature *Zea mays* leaves (closed circles). Panels A and C show the distributions of the peak wavelengths and the widths of microscopic fluorescence spectra, respectively: A-1 and C-1 for the mature *Zea mays* leaves, A-2 and C-2 for the 3-h greening *Zea mays* leaves, and A-3 and C-3 for the 1-h greening *Zea mays* leaves.

Table 1
statistics of the spectral properties of greening and mature *Zea mays* leaves.

	1-h greening (143)	3-h greening (126)	Mature (47)
Average peak wavelength [nm]	681.0 ± 1.4	682.7 ± 1.0	684.4 ± 0.8
Average band width [nm]	13.4 ± 2.9	14.3 ± 1.7	14.1 ± 0.7

The values in parenthesis are the sample sizes.

clearly show that the large variability of spectral profiles in 1-h greening leaves decreases as the greening proceeds. The averaged peak wavelengths, band widths, and their dispersions are listed in Table 1. It is clear that the 1-h greening leaf displayed the largest dispersions for both the band width and the peak wavelength. The points with open circles in Fig. 7(B) for the 1-h greening can be roughly divided into two groups. One has an averaged peak wavelength at 679 nm and band width of 16 nm (surrounded with the dashed ellipse), and the other has an averaged peak wavelength at 682 nm and band width of 12 nm (surrounded with the dotted ellipse).

The fluorescence-ratio maps of the 1-h greening leaves in Figs. 4 and S4 showed that microscopic fluorescence spectra with peaks at shorter wavelengths tended to be observed in the BS cells neighboring the VB. Exceptions to the above tendency are seen, for example, at around the leaf-surface, in which the ratios of longer- to shorter-wavelength-emitting fluorescence intensities are as low as in the VB-neighboring regions. It is not clear what is the origin of the low ratio values around the leaf surface. Higher intensity of the greening-inducing light might cause the exceptional low ratio values in the region near the surface. The above results, albeit the exceptions and the small sampling size, are consistent with a report by Marchand et al. [33], in which the isolated BS cells from etiolated *Zea mays* showed the fluorescence maxima at around 677 nm 90 min after the flash illumination, while the MS cells showed the fluorescence maxima at around 681 nm in the same condition. The former 677-nm emitting pigment form seems to correspond to the Chl-*a* group surrounded with the dashed ellipse in Fig. 7(B), and the latter, to that surrounded with the dotted ellipse. Mixtures of fluorescence from different forms may result in a slight shift of the fluorescence maximum for each Chl-*a* group from the reported value in the literature [33]. Marchand et al. interpreted that the fluorescence spectra with the maximum at 681 nm are emitted from the precursors to PS II, which develop after the long-wavelength (693 nm)-emitting form induced 15 min after flash irradiation to an etiolated plant. The 693-nm-emitting form was interpreted to be the intermediate on the pathway leading to the PS II assembly [17], and was missing in BS cells of the etiolated *Zea mays* [33].

The 679-nm-emitting Chl-*a* form (the group surrounded with the dashed ellipse in Fig. 7(B)) is accumulated mainly in the BS cells. This assignment is based on the ratio maps in Figs. 4 and S4, showing the accumulation of the shorter-wavelength-emitting form near the VB. Here, we tentatively assign this form to be related to intermediates leading to the PS I assembly. There have been only a few reports about the assembly intermediates of PS I so far. Ycf4 has been considered to be an essential component assisting the assembly of PS I in a green alga, *C. reinharditi* [20,23,42]. Ozawa et al. purified a large (>1500 kD) Ycf4-contanining complex containing the PS I polypeptides, PsaA to PsaF, and several other subunits [23]. They proposed a model of PS I assembly in *C. reinharditi*, in which the large complex containing Ycf4 is assumed to play a key role as a molecular chaperone. It is an important future work to compare the optical properties of the PS I assembly intermediates in *C. reinharditi* with those observed in the BS cells of the 1-h greening leaves in the present study.

The 679-nm-emitting form, showing higher accumulation in the BS cells, had a broader band width than the 682-nm-emitting one that was mainly assigned to the MS cells. This is a puzzling finding, as the spectral band widths were expected to be broader for the MS than for the BS cells because the former contain mixed contributions from the precursors to both PS I and PS II while the latter contain those mainly from the PS I precursors. A possible explanation for the observed broader spectral width for the BS cells is that the PS I intermediates had broader fluorescence spectral widths as well as much lower fluorescence quantum yield than the PS II intermediates. Due to the low fluorescence quantum yield of the PS I intermediates, the fluorescence from the MS cells is dominated by the contribution from the PS II intermediates having smaller fluorescence spectral widths.

5. Conclusions

In the present study, we applied for the first time the cryogenic confocal microspectroscopy to observations of *Zea mays* leaves under the greening process. The study revealed larger sizes of the fluorescence spots attributed to $PChld_{632}$ than those attributed to $PChld_{655}$. Thus, the assignments of $PChld_{632}$ and $PChld_{655}$, respectively, to PT and PLB could be validated by the present *in vivo* measurement. We also succeeded in carrying out *in vivo* spectroscopic measurements of the cell differentiation process in a C4-plant *Zea mays* through the greening process. The fluorescence spectroscopic properties were confirmed to be different between the BS and MS cells already in the 1-h greening stage. The Chl-*a* forms observed mainly in the BS cells might be attributable to the PS I precursors.

Acknowledgements

This work was supported in part by Grants-in-Aid for Scientific Research (No. 21750017), the 21st COE program for "the origin of the universe and matter" from the Japanese Ministry of Education, Science, Sports, and Culture (MEXT), and the Japan Society for the Promotion of Science (JSPS).

Appendix A. Supplementary data

Supplementary data to this article can be found online at http://dx.doi.org/10.1016/j.bbabio.2013.02.001.

References

[1] L.A. Eichacker, B. Muller, M. Helfrich, Stabilization of the chlorophyll binding apoproteins, P700, CP47, CP43, D2, and D1, by synthesis of Zn-pheophytin a in intact etioplasts from barley, FEBS Lett. 395 (1996) 251–256.
[2] B. Muller, L.A. Eichacker, Assembly of the D1 precursor in monomeric photosystem II reaction center precomplexes precedes chlorophyll a-triggered accumulation of reaction center II in barley etioplasts, Plant Cell 11 (1999) 2365–2377.
[3] In: R.R. Wise, J.K. Hoober (Eds.), The Structure and Function of Plastids, Springer, Dordrecht, 2006.
[4] E. Kanervo, M. Singh, M. Suorsa, V. Paakkarinen, E. Aro, N. Battchikova, E.M. Aro, Expression of protein complexes and individual proteins upon transition of etioplasts to chloroplasts in pea (Pisum sativum), Plant Cell Physiol. 49 (2008) 396–410.
[5] S. Klein, G. Bryan, L. Bogorad, Early stages in development of plastid fine structure in red + far-red light, J. Cell Biol. 22 (1964) 433–442.
[6] B.E.S. Gunning, Greening process in plastids.1. Structure of prolamellar body, Protoplasma 60 (1965) 111–130.
[7] S. Klein, J.A. Schiff, Correlated appearance of prolamellar bodies, protochlorophyll(ide) species, and Shibata shift during development of bean etioplasts in dark, Plant Physiol. 49 (1972) 619–626.
[8] R.O. Mackender, Etioplast development in dark-grown leaves of *Zea mays*-L, Plant Physiol. 62 (1978) 499–505.
[9] D. Robertson, W.M. Laetsch, Structure and function of developing barley plastids, Plant Physiol. 54 (1974) 148–159.
[10] C. Sundqvist, C. Dahlin, With chlorophyll pigments from prolamellar bodies to light-harvesting complexes, Physiol. Plant. 100 (1997) 748–759.
[11] K. Shibata, Spectroscopic studies on chlorophyll formation in intact leaves, J. Biochem. 44 (1957) 147–173.
[12] B. Schoefs, The protochlorophyllide–chlorophyllide cycle, Photosynth. Res. 70 (2001) 257–271.
[13] B. Schoefs, Protochlorophyllide reduction — what is new in 2005? Photosynthetica 43 (2005) 329–343.
[14] A. Lindsten, M. Ryberg, C. Sundqvist, The polypeptide composition of highly purified prolamellar bodies and prothylakoids from wheat (*Triticum aestivum*) as revealed by silver staining, Physiol. Plant. 72 (1988) 167–176.

[15] B. Boddi, M. Ryberg, C. Sundqvist, Identification of 4 universal protochlorophyllide forms in dark-grown leaves by analyses of the 77-K fluorescence emission-spectra, J. Photochem. Photobiol. B 12 (1992) 389–401.
[16] P. Mathis, K. Sauer, Chlorophyll formation in greening bean-leaves during early stages, Plant Physiol. 51 (1973) 115–119.
[17] F. Franck, P. Eullaffroy, R. Popovic, Formation of long-wavelength chlorophyllide (Chlide695) is required for the assembly of Photosystem II in etiolated barley leaves, Photosynth. Res. 51 (1997) 107–118.
[18] P. Mulo, S. Sirpiö, M. Suorsa, E.M. Aro, Auxiliary proteins involved in the assembly and sustenance of Photosystem II, Photosynth. Res. 98 (2008) 489–501.
[19] P.J. Nixon, F. Michoux, J.F. Yu, M. Boehm, J. Komenda, Recent advances in understanding the assembly and repair of photosystem II, Ann. Bot. 106 (2010) 1–16.
[20] M.A. Schöttler, C.A. Albus, R. Bock, Photosystem I: its biogenesis and function in higher plants, J. Plant Physiol. 168 (2011) 1452–1461.
[21] A. Rokka, M. Suorsa, A. Saleem, N. Battchikova, E.M. Aro, Synthesis and assembly of thylakoid protein complexes: multiple assembly steps of Photosystem II, Biochem. J. 388 (2005) 159–168.
[22] S. Ozawa, J. Nield, A. Terao, E.J. Stauber, M. Hippler, H. Koike, J.D. Rochaix, Y. Takahashi, Biochemical and structural studies of the large ycf4-Photosystem I assembly complex of the green alga *Chlamydomonas reinhardtii*, Plant Cell 21 (2009) 2424–2442.
[23] S. Ozawa, T. Onishi, Y. Takahashi, Identification and characterization of an assembly intermediate subcomplex of Photosystem I in the green alga *Chlamydomonas reinhardtii*, J. Biol. Chem. 285 (2010) 20072–20079.
[24] L.A. Blomqvist, M. Ryberg, C. Sundqvist, Proteomic analysis of highly purified prolamellar bodies reveals their significance in chloroplast development, Photosynth. Res. 96 (2008) 37–50.
[25] E.A. van Spronsen, V. Sarafis, G.J. Brakenhoff, H.T.M. Vandervoort, N. Nanninga, 3-Dimensional structure of living chloroplasts as visualized by confocal scanning laser microscopy, Protoplasma 148 (1989) 8–14.
[26] S.G. Chuartzman, R. Nevo, E. Shimoni, D. Charuvi, V. Kiss, I. Ohad, V. Brumfeld, Z. Reich, Thylakoid membrane remodeling during state transitions in *Arabidopsis*, Plant Cell 20 (2008) 1029–1039.
[27] M. Hasegawa, T. Shiina, M. Terazima, S. Kumazaki, Selective excitation of photosystems in chloroplasts inside plant leaves observed by near-infrared laser-based fluorescence spectral microscopy, Plant Cell Physiol. 51 (2010) 225–238.
[28] S. Pancaldi, C. Baldisserotto, L. Ferroni, A. Bonora, M.P. Fasulo, Room temperature microspectrofluorimetry as a useful tool for studying the assembly of the PSII chlorophyll–protein complexes in single living cells of etiolated Euglena *gracilis Klebs* during the greening process, J. Exp. Bot. 53 (2002) 1753–1763.
[29] K.A. Kristiansen, A. Khrouchtchova, A. Stenbaek, A. Schulz, P.E. Jensen, Non-invasive method for *in vivo* detection of chlorophyll precursors, Photochem. Photobiol. Sci. 8 (2009) 279–286.
[30] H. Egneus, G. Sellden, S. Reftel, Appearance and development of photosynthetic activity in etiolated barley leaves and isolated etio-chloroplasts, Physiol. Plant. 27 (1972) 48–55.
[31] M. Plesnicar, D.S. Bendall, Photochemical activities and electron carriers of developing barley leaves, Biochem. J. 136 (1973) 803–812.
[32] K. Ohashi, A. Murakami, A. Tanaka, H. Tsuji, Y. Fujita, Developmental-changes in amounts of thylakoid components in plastids of barley leaves, Plant Cell Physiol. 33 (1992) 371–377.
[33] M. Marchand, D. Dewez, F. Franck, R. Popovic, Protochlorophyllide phototransformation in the bundle sheath cells of *Zea mays*, J. Photochem. Photobiol. B 75 (2004) 73–80.
[34] B.W. Dreyfuss, J.P. Thornber, Organization of the light-harvesting complex of Photosystem I and its assembly during plastid development, Plant Physiol. 106 (1994) 841–848.
[35] E. Wientjes, R. Croce, The light-harvesting complexes of higher-plant Photosystem I: Lhca1/4 and Lhca2/3 form two red-emitting heterodimers, Biochem. J. 433 (2011) 477–485.
[36] R. Croce, G. Zucchelli, F.M. Garlaschi, R.C. Jennings, A thermal broadening study of the antenna chlorophylls in PSI-200, LHCI, and PSI core, Biochem. 37 (1998) 17355–17360.
[37] R.J. van Dorssen, J.J. Plijter, J.P. Dekker, A. Denouden, J. Amesz, H.J. Vangorkom, Spectroscopic properties of chloroplast grana membranes and of the core of Photosystem II, Biochim. Biophys. Acta 890 (1987) 134–143.
[38] R.J. van Dorssen, J. Breton, J.J. Plijter, K. Satoh, H.J. Vangorkom, J. Amesz, Spectroscopic properties of the reaction center and of the 47 kDa chlorophyll protein of Photosystem II, Biochim. Biophys. Acta 893 (1987) 267–274.
[39] G.Z. Shen, W.F.J. Vermaas, Mutation of chlorophyll ligands in the chlorophyll-binding CP47-protein as studied in a *Synechocystis* sp PCC6803 Photosystem I-less background, Biochem. 33 (1994) 7379–7388.
[40] F.L. de Weerd, M.A. Palacios, E.G. Andrizhiyevskaya, J.P. Dekker, R. van Grondelle, Identifying the lowest electronic states of the chlorophylls in the CP47 core antenna protein of Photosystem II, Biochem. 41 (2002) 15224–15233.
[41] E.G. Andrizhiyevskaya, A. Chojnicka, J.A. Bautista, B.A. Diner, R. van Grondelle, J.P. Dekker, Origin of the F685 and F695 fluorescence in Photosystem II, Photosynth. Res. 84 (2005) 173–180.
[42] E. Boudreau, Y. Takahashi, C. Lemieux, M. Turmel, J.D. Rochaix, The chloroplast ycf3 and ycf4 open reading frames of *Chlamydomonas reinhardtii* are required for the accumulation of the Photosystem I complex, EMBO J. 16 (1997) 6095–6104.